Inorg. Chem. **2005**, *44*, 5571–5579

Oxalate-Bridged Dinuclear M_2 Units: Dimers of Dimers, Cyclotetramers, and Extended Sheets (M = Mo, W, Tc, Ru, and Rh)

Bruce E. Bursten,* Malcolm H. Chisholm,* and Jason S. D'Acchioli

Department of Chemistry, The Ohio State University, 100 West 18th Avenue, Columbus, Ohio 43210

Received January 13, 2005

The electronic structures of D_{4h}-$M_2(O_2CH)_4$ and the oxalate-bridged complexes D_{2h}-$[(HCO_2)_3M_2]_2(\mu$-$O_2CCO_2)$ and D_{4h}-$[(HCO_2)_2M_2]_4(\mu$-$O_2CCO_2)_4$ have been investigated by a symmetry analysis of their MM and oxalate-based frontier orbitals, as well as by electronic structure calculations on the model formate complexes (M = Mo and W $\{d^4$-$d^4\}$, Tc, Ru $\{d^6$-$d^6\}$, and Rh $\{d^7$-$d^7\}$). Significant changes in the ordering, interactions, and electronic occupation of the molecular orbitals (MOs) arise through both the progression from d^4 to d^7 metals and the change from second to third row transition metals. For M = Mo and W, the highest-occupied orbitals are δ based, while the lowest-unoccupied orbitals are oxalate π^* based; for M = Tc, the highest-occupied orbitals are an energetically tight δ^*-based set of MOs, while the lowest-unoccupied orbitals are MM-based π^*. For both Ru and Rh, the highest-occupied MOs are the MM π^* and δ^*, respectively, while the lowest-unoccupied MOs, in both instances, are MM-based σ^*. With the exception of M = Ru, all of the complexes are closed shell. From the progression $M_2 \rightarrow [M_2]_2 \rightarrow [M_2]_4$, we can envision the nature of bandlike structures for a 2-dimensional square grid of formula $[M_2(\mu$-$O_2CCO_2)]_\infty$. Only for Mo and W oxalates should good electronic communication between MM centers generate a band of significant width to lead to metallic conductivity upon oxidation.

Introduction

Dicarboxylate-based ligands have been employed to link dinuclear transition metal centers yielding what may be described as dimers of dimers, cyclotrimers or molecular triangles, and cyclotetramers or molecular squares, as well as extended lattice structures.[1−13] When the dicarboxylate linker contains an extended π system, these architectures can lead to the electronic coupling of the MM centers, as can be seen from the work of Cotton et al. (M = Mo, Ru, Rh)[14−17] and from the work in this laboratory (M = Mo, W).[5,14,18−25] From the work of Lehn, Yaghi, Mori, and their

* To whom correspondence should be addressed. E-mail: chisholm@chemistry.ohio-state.edu (M.H.C.); bursten@chemistry.ohio-state.edu (B.E.B.).

(1) Bonar-Law, R. P.; McGrath, T. D.; Singh, N.; Bickley, J. F.; Steiner, A. *Chem. Commun.* **1999**, 2457.
(2) Cotton, F. A.; Daniels, L. M.; Lin, C.; Murillo, C. A. *J. Am. Chem. Soc.* **1999**, *121*, 4538.
(3) Bickley, J. F.; Bonar-Law, R. P.; Femoni, C.; MacLean, E. J.; Steiner, A.; Teat, S. J. *J. Chem. Soc., Dalton Trans.* **2000**, 4025.
(4) Bera, J. K.; Smucker, B. W.; Walton, R. A.; Dunbar, K. R. *Chem. Commun.* **2001**, 2562.
(5) Bursten, B. E.; Chisholm, M. H.; Hadad, C. M.; Li, J.; Wilson, P. J. *Isr. J. Chem.* **2001**, *41*, 187.
(6) Cotton, F. A.; Daniels, L. M.; Lin, C.; Murillo, C. A.; Yu, S.-Y. *J. Chem. Soc., Dalton Trans.* **2001**, 502.
(7) Cotton, F. A.; Lin, C.; Murillo, C. A. *Chem. Commun.* **2001**, 11.
(8) Cotton, F. A.; Lin, C.; Murillo, C. A. *Acc. Chem. Res.* **2001**, *34*, 759.
(9) Cotton, F. A.; Lin, C.; Murillo, C. A. *Inorg. Chem.* **2001**, *40*, 478.
(10) Cotton, F. A.; Lin, C.; Murillo, C. A. *Proc. Natl. Acad. Sci. U.S.A.* **2002**, *99*, 4810.
(11) Angaridis, P.; Berry, J. F.; Cotton, F. A.; Murillo, C. A.; Wang, X. *J. Am. Chem. Soc.* **2003**, *125*, 10327.
(12) Bera, J. K.; Bacsa, J.; Smucker, B. W.; Dunbar, K. R. *Eur. J. Inorg. Chem.* **2004**, 368.
(13) Cotton, F. A.; Murillo, C. A.; Wang, X.; Yu, R. *Inorg. Chem.* **2004**, *43*, 8394.
(14) Chisholm, M. H. *J. Organomet. Chem.* **2002**, *641*, 15.
(15) Cotton, F. A. *J. Am. Chem. Soc.* **2003**, *125*, 5436.
(16) Cotton, F. A.; Donahue, J. P.; Murillo, C. A.; Perez, L. M. *J. Am. Chem. Soc.* **2003**, *125*, 5486.
(17) Berry, J. F.; Cotton, F. A.; Lei, P.; Lin, C.; Murillo, C. A.; Villagran, D. *Inorg. Chem. Commun.* **2004**, *7*, 9.
(18) Cayton, R. H.; Chisholm, M. H.; Huffman, J. C.; Lobkovsky, E. B. *J. Am. Chem. Soc.* **1991**, *113*, 8709.
(19) Chisholm, M. H. *Acc. Chem. Res.* **2000**, *33*, 53.
(20) Bursten, B. E.; Chisholm, M. H.; Clark, R. J. H.; Firth, S.; Hadad, C. M.; MacIntosh, A. M.; Wilson, P. J.; Woodward, P. M.; Zaleski, J. M. *J. Am. Chem. Soc.* **2002**, *124*, 3050.
(21) Bursten, B. E.; Chisholm, M. H.; Clark, R. J. H.; Firth, S.; Hadad, C. M.; Wilson, P. J.; Woodward, P. M.; Zaleski, J. M. *J. Am. Chem. Soc.* **2002**, *124*, 12244.
(22) Byrnes, M. J.; Chisholm, M. H. *Chem. Commun.* **2002**, 2040.
(23) Chisholm, M. H.; Pate, B. D.; Wilson, P. J.; Zaleski, J. M. *Chem. Commun.* **2002**, 1084.
(24) Chisholm, M. H. *J. Chem. Soc., Dalton Trans.* **2003**, 3821.
(25) Byrnes, M. J.; Chisholm, M. H.; Clark, R. J. H.; Gallucci, J. C.; Hadad, C. M.; Patmore, N. J. *Inorg. Chem.* **2004**, *43*, 6334.

10.1021/ic050053n CCC: $30.25
Published on Web 07/01/2005

respective co-workers, it is clear that such extended network inorganic/organic hybrid materials can be prepared to accommodate guest molecules within their channels.[26−39]

The key to understanding the nature of electronic coupling between M_2 centers lies in an examination of their molecular orbital (MO) diagrams. The clue as to whether the system will be efficiently coupled lies in the interaction of the M_2 δ-based orbitals and the bridge π orbitals. A direct measure of this interaction is the degree of dispersion between the M_2 δ orbitals, *after* favorable energetic and correct symmetry interactions (vide infra). In essence, the larger the dispersion between the M_2 δ orbitals, the greater the interaction with the bridging ligand; electronic coupling will thus be more likely. However, if there is less dispersion between the M_2 δ orbitals, we would expect less interaction with the bridging ligands and less electronic coupling between centers.

The simplest dicarboxylate bridge is oxalate, and, as we have described elsewhere, it proves an efficient bridge for electronic communication between MM quadruply bonded units.[5,20,23] With the intent of building a knowledge of the electronic structures of these extended materials, we have examined the bonding in a series of molecular model compounds containing M_2^{4+} units, starting with the tetraformates $M_2(O_2CH)_4$, followed by the oxalate-bridged dimer of dimers $[(HCO_2)_3M_2]_2(\mu\text{-}O_2CCO_2)$ with D_{2h} symmetry and the molecular squares $[(HCO_2)_3M_2]_4(\mu\text{-}O_2CCO_2)_4$ with D_{4h} symmetry (Figure 1). In this paper, we have built these systems up from a symmetry analysis of the frontier orbitals of the MM fragments and the oxalate π system for the metals M = Mo and W (d^4), M = Tc (d^5), M = Ru (d^6), and M = Rh (d^7). For the molecules D_{4h}-$M_2(O_2CH)_4$, D_{2h}-$[(HCO_2)_3M_2]_2(\mu\text{-}O_2CCO_2)$, and D_{4h}-$[(HCO_2)_2M_2]_4(\mu\text{-}O_2CCO_2)_4$ we have also carried out electronic structure calculations employing density functional theory. This work provides the first step in examining the electronic structures of related oxalate-bridged dimers of dimers and molecular squares, and from these calculations, we can anticipate the electronic structure of the 2-D extended square grid structures for materials of formula $[M_2(\mu\text{-}O_2CCO_2)]_\infty$.

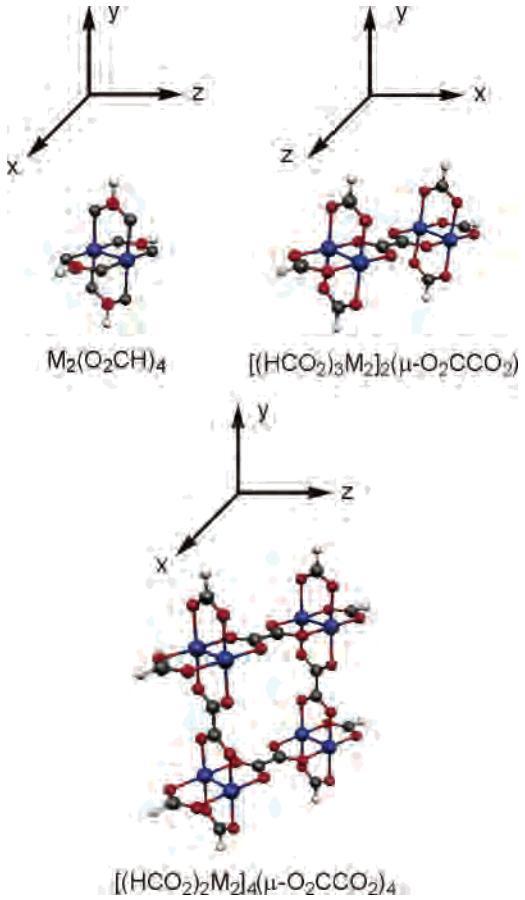

Figure 1. The formate model complexes considered in this study (Red = oxygen, gray = carbon, blue = transition metal, and white = hydrogen). The orientation of each complex in the calculations is indicated by the Cartesian axes.

Computational Details

Scalar relativistic density functional theory (DFT) calculations have been performed using the Amsterdam Density Functional (ADF 2002.03) code[40] with the inclusion of the generalized gradient approach of Perdew and Wang (PW91).[41−45] The [$1s^2$] cores for C and O, the [$1s^2$-$4p^6$] cores for Mo, Tc, Ru, and Rh, and the [$1s^2$-

(26) Takamizawa, S.; Mori, W.; Furihata, M.; Takeda, S.; Yamaguchi, K. *Inorg. Chim. Acta* **1998**, *283*, 268.
(27) Takamizawa, S.; Yamaguchi, K.; Mori, W. *Inorg. Chem. Commun.* **1998**, *1* 177.
(28) Mori, W.; Takamizawa, S. *J. Solid State Chem.* **2000**, *152*, 120.
(29) Takamizawa, S.; Furihata, M.; Takeda, S.; Yamaguchi, K.; Mori, W. *Polym. Adv. Technol.* **2000**, *11*, 840.
(30) Eddaoudi, M.; Moler, D. B.; Li, H.; Chen, B.; Reineke, T. M.; O'Keeffe, M.; Yaghi, O. M. *Acc. Chem. Res.* **2001**, *34*, 319.
(31) Seki, K.; Takamizawa, S.; Mori, W. *Chem. Lett.* **2001**, 122.
(32) Mori, W.; Takamizawa, S. Suprazeolite Microporous Materials of Metal Carboxylates. In *Organometallic Conjugation*; Nakamura, A., Ueyama, N., Yamaguchi, K., Eds.; Springer Series in Chemical Physics; Springer: New York, 2002; Vol. 73, p 179.
(33) Rosi, N. L.; Eddaoudi, M.; Kim, J.; O'Keeffe, M.; Yaghi, O. M. *Cryst. Eng. Comm.* **2002**, *4*, 401.
(34) Takamizawa, S.; Hiroki, T.; Nakata, E.-I.; Mochizuki, K.; Mori, W. *Chem. Lett.* **2002**, 1208.
(35) Ohmura, T.; Mori, W.; Hasegawa, M.; Takei, T.; Ikeda, T.; Hasegawa, E. *Bull. Chem. Soc. Jpn.* **2003**, *76*, 1387.
(36) Ohmura, T.; Mori, W.; Hiraga, H.; Ono, M.; Nishimoto, Y. *Chem. Lett.* **2003**, *32*, 468.
(37) Yaghi, O. M.; O'Keeffe, M.; Ockwig, N. W.; Chae, H. K.; Eddaoudi, M.; Kim, J. *Nature (London)* **2003**, *423*, 705.
(38) Mori, W.; Takamizawa, S.; Kato, C. N.; Ohmura, T.; Sato, T. *Microporous Mesoporous Mater.* **2004**, *73*, 31.
(39) Ruben, M.; Rojo, J.; Romero-Salguero, F. J.; Uppadine, L. H.; Lehn, J.-M. *Angew. Chem., Int. Ed.* **2004**, *43*, 3644.
(40) Baerends, E. J.; Autschbach, J. A.; Bérces, A.; Bo, C.; Boerrigter, P. M.; Cavallo, L.; Chong, D. P.; Deng, L.; Dickson, R. M.; Ellis, D. E.; Fan, L.; Fischer, T. H.; Fonseca Guerra, C. F.; van Gisbergen, S. J. A.; Groeneveld, J. A.; Gritsenko, O. V.; Grüning, M.; Harris, F. E.; van den Hoek, P.; Jacobsen, H.; van Kessel, G.; Kootstra, F.; van Lenthe, E.; Osinga, V. P.; Patchkovskii, S.; Philipsen, P. H. T.; Post, D.; Pye, C. C.; Ravenek, W.; Ros, P.; Schipper, P. R. T.; Schreckenbach, G.; Snijders, J. G.; Sola, M.; Swart, M.; Swerhone, D.; te Velde, G.; Vernooijs, P.; Versluis, L.; Visser, O.; van Wezenbeek, E.; Wiesenekker, G.; Wolff, S. K.; Woo, T. K.; Ziegler, T. *ADF*, 2002.03; Scientific Computing & Modelling: Amsterdam, The Netherlands, 2003, www.scm.com.
(41) Perdew, J. P., In *Electronic Structure of Solids*; Ziesche, P., Eschrig, H., Eds.; Akademie Verlag: Berlin, 1991; p 11.
(42) Perdew, J. P.; Chevary, J. A.; Vosko, S. H.; Jackson, K. A.; Pederson, M. R.; Singh, D. J.; Fiolhais, C. *Phys. Rev. B: Condens. Matter Mater. Phys.* **1992**, *46*, 6671.
(43) Perdew, J. P.; Chevary, J. A.; Vosko, S. H.; Jackson, K. A.; Pederson, M. R.; Singh, D. J.; Fiolhais, C. *Phys. Rev. B: Condens. Matter Mater. Phys.* **1993**, *48*, 4978.
(44) Perdew, J. P.; Burke, K.; Wang, Y. *Phys. Rev. B: Condens. Matter Mater. Phys.* **1996**, *54*, 16533.

Table 1. Irreducible Representations Spanned by the Metal-Based Orbitals in $M_2(O_2CH)_4$ (D_{4h}), $[(HCO_2)_3M_2]_2(\mu\text{-}O_2CCO_2)$ (D_{2h}), and $[(HCO_2)_3M_2]_4(\mu\text{-}O_2CCO_2)_4$ (D_{4h})[a]

metal-based orbitals	M_2 (D_{4h})	$[M_2]_2$ (D_{2h})	$[M_2]_4$ (D_{4h})
σ	a_{1g}	$a_g + b_{1u}$	$a_{1g} + b_{2g} + e_u$
π	e_u	$a_g + b_{3g} + b_{1u} + b_{2u}$	$a_{1g} + a_{2g} + b_{1g} + b_{2g} + 2e_u$
δ	b_{2g}	$b_{3g} + b_{2u}$	$a_{1g} + b_{2g} + e_u$
δ^*	b_{1u}	$b_{1g} + a_u$	$e_g + a_{2u} + b_{1u}$
π^*	e_g	$b_{1g} + b_{2g} + a_{1u} + b_{3u}$	$a_{1u} + a_{2u} + b_{1u} + b_{2u} + 2e_g$
σ^*	a_{2u}	$b_{2g} + b_{3u}$	$e_g + a_{2u} + b_{1u}$

[a] While there are no degenerate representations in D_{2h} symmetry, the d orbitals which make up the π molecular orbitals (d_{xz}, d_{yz}) are grouped together for the sake of consistency.

$5p^6$] cores for W were frozen. It should be noted that paddle wheel-based systems of Re(II) were not considered because of convergence problems in systems of the form D_{2h}-$[(HCO_2)_3M_2]_2(\mu\text{-}O_2CCO_2)$ and D_{4h}-$[(HCO_2)M_2]_4(\mu\text{-}O_2CCO_2)_4$. Slater-type-orbital (STO) basis sets of triple-ζ quality with f-type polarization functions were used for the valence orbitals of all transition metal atoms. STO basis sets of double-ζ quality with d-type polarization functions were used for C and O. A STO basis set of double-ζ quality with p-type polarization functions was used for H. The default convergence criteria were used for each geometry optimization with the exception of the convergence gradient, which was tightened from 0.01 to 0.001. The structures of the calculated species were fully optimized in their respective point groups with the inclusion of scalar relativistic effects using the ZORA formalism.[46−50] Vibrational frequency analyses were not performed on these systems to verify if the structures were a local minimum on the potential energy surface. This approach can be rationalized by the desire to maintain the highest idealized symmetry possible for the structures in this study, i.e., D_{2h} and D_{4h}, for the purpose of orbital analysis. MO isosurfaces were generated using the program Molekel.[51]

Computational Results

Setting the Stage: Frontier Molecular Orbital Interactions in D_{4h}-$M_2(O_2CH)_4$ Dimers. It is instructive to start this exercise by examining the key orbital interactions that result from the linking of MM units having a paddle wheel core via the oxalate bridge. The MM bonding manifold of orbitals is well-known as σ, π, δ, δ^*, π^*, and σ^*[52] and, in D_{4h} symmetry, is spanned by the irreducible representations listed in Table 1. Orbital plots illustrating a typical MM manifold are shown for $Mo_2(O_2CH_4)_4$ in Figure 2.

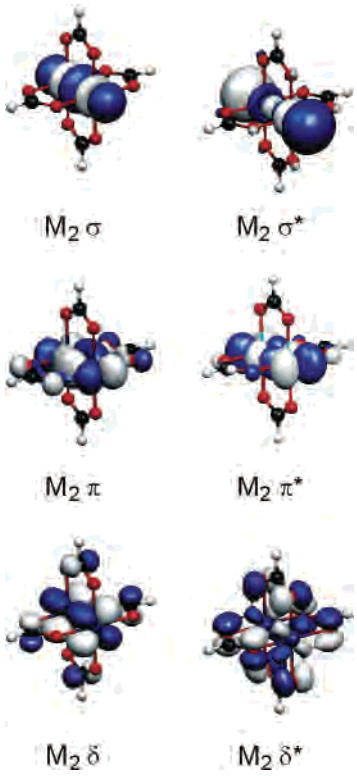

Figure 2. Molecular orbital isosurfaces for $Mo_2(O_2CH)_4$. The frontier MOs shown illustrate the typical M−M interactions in quadruply bonded systems. Only one of the degenerate π and π^* orbitals is shown for simplicity (isosurface cutoff value = 0.04).

While studies on $M_2(O_2CH)_4$ (M = Mo, W, Tc, Ru, and Rh) are known,[18,53−69] it was instructive to evaluate all model complexes using the same level of theory. This consistency is crucial for making meaningful comparisons upon going from the model compounds D_{4h}-$M_2(O_2CH)_4$ to D_{2h}-$[(HCO_2)_3M_2]_2(\mu\text{-}O_2CCO_2)$ and D_{4h}-$[(HCO_2)M_2]_4(\mu\text{-}O_2CCO_2)_4$.

We begin our discussion with the simplest system possible, i.e., the dimer $M_2(O_2CH)_4$ (M = Mo, W, Tc, Ru, and Rh). Figures 3 and 4 show qualitative frontier MO diagrams for

(45) Burke, K.; Perdew, J. P.; Wang, Y. Derivation of a Generalized Gradient Approximation: The PW91 Density Functional. In *Electronic Density Functional Theory: Recent Progress and New Directions*, Proceedings of the International Workshop on Electronic Density Functional Theory: Recent Progress and New Directions, Nathan, Australia, July 14−19 1996; Dobson, J. F., Vignale, G., Das, M. P., Eds; Plenum: New York, 1998; p 81.
(46) van Lenthe, E.; Baerends, E. J.; Snijders, J. G. *J. Chem. Phys.* **1993**, *99*, 4597.
(47) van Lenthe, E.; Baerends, E. J.; Snijders, J. G. *J. Chem. Phys.* **1994**, *101*, 9783.
(48) van Lenthe, E.; Snijders, J. G.; Baerends, E. J. *J. Chem. Phys.* **1996**, *105*, 6505.
(49) van Lenthe, E.; van Leeuwen, R.; Baerends, E. J.; Snijders, J. G. *Int. J. Quantum Chem.* **1996**, *57*, 281.
(50) van Lenthe, E.; Ehlers, A.; Baerends, E. J. *J. Chem. Phys.* **1999**, *110*, 8943.
(51) Flükiger, P. F.; Portmann, S. *Molekel*, 4.3; Swiss National Supercomputing Centre: Geneva, 2002, www.cscs.ch/molekel/.
(52) Cotton, F. A.; Walton, R. A. *Multiple Bonds Between Metal Atoms*, 2nd ed.; Clarendon Press: Oxford, U.K., 1993.
(53) Norman, J. G., Jr.; Kolari, H. J. *J. Chem. Soc., Chem. Commun.* **1975**, 649.
(54) Norman, J. G., Jr.; Kolari, H. J.; Gray, H. B.; Trogler, W. C. *Inorg. Chem.* **1977**, *16*, 987.
(55) Benard, M. *J. Am. Chem. Soc.* **1978**, *100*, 2354.
(56) Norman, J. G., Jr.; Kolari, H. J. *J. Am. Chem. Soc.* **1978**, *100*, 791.
(57) Norman, J. G., Jr.; Renzoni, G. E.; Case, D. A. *J. Am. Chem. Soc.* **1979**, *101*, 5256.
(58) Nakatsuji, H.; Ushio, J.; Kanda, K.; Onishi, Y.; Kawamura, T.; Yonezawa, T. *Chem. Phys. Lett.* **1981**, *79*, 299.
(59) Atha, P. M.; Campbell, J. C.; Garner, C. D.; Hillier, I. H.; MacDowell, A. A. *J. Chem. Soc., Dalton Trans.* **1983**, 1085.
(60) Manning, M. C.; Holland, G. F.; Ellis, D. E.; Trogler, W. C. *J. Phys. Chem.* **1983**, *87*, 3083.
(61) Nakatsuji, H.; Onishi, Y.; Ushio, J.; Yonezawa, T. *Inorg. Chem.* **1983**, *22*, 1623.
(62) Braydich, M. D.; Bursten, B. E.; Chisholm, M. H.; Clark, D. L. *J. Am. Chem. Soc.* **1985**, *107*, 4459.
(63) Stroemberg, A.; Pettersson, L. G. M.; Wahlgren, U. *Chem. Phys. Lett.* **1985**, *118*, 389.
(64) Ziegler, T. *J. Am. Chem. Soc.* **1985**, *107*, 4453.
(65) Sierraalta, A. *Chem. Phys. Lett.* **1994**, *227*, 557.
(66) Cotton, F. A.; Feng, X. *J. Am. Chem. Soc.* **1997**, *119*, 7514.
(67) Cotton, F. A.; Feng, X. *J. Am. Chem. Soc.* **1998**, *120*, 3387.
(68) Estiu, G.; Cukiernik, F. D.; Maldivi, P.; Poizat, O. *Inorg. Chem. Commun.* **1999**, *38*, 3030.
(69) Petrie, S.; Stranger, R. *Inorg. Chem.* **2004**, *43*, 2597.

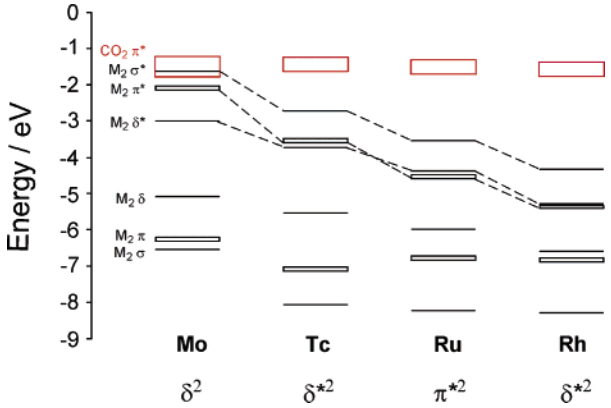

Figure 3. Frontier MO diagrams for second row transition metal $M_2(O_2CH)_4$ complexes (M = Mo, Tc, Ru, or Rh). The occupation of the HOMO is indicated below the metal of interest. Note the crossing of the δ^* and π^* MOs upon moving from Tc to Ru (see text).

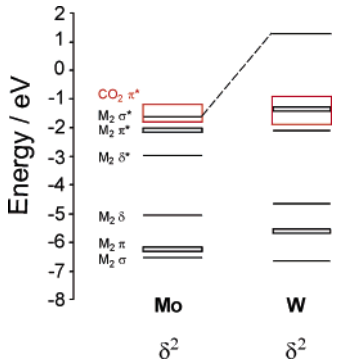

Figure 4. Frontier MO diagram for third row transition metal complex $W_2(O_2CH)_4$ as compared to that of $Mo_2(O_2CH)_4$. The occupation of the HOMO is indicated below the metal.

each of the calculated species, separated according to the metal's position as either a second or third row transition metal. There are two salient features in these diagrams. The first deals with the periodic change in the energy of the frontier orbitals upon going from one metal to another across a row and then from one metal to another down a period. The second, more intriguing, observation comes from noting the changes in the energy of the HOMO as one progresses from a $\delta^4-\delta^4$ system to a $\delta^7-\delta^7$ system.

As one moves from Mo to Rh, it is readily apparent that the energies of the MM-based MOs decrease, while those of the CO_2 π^*-based orbitals remain fairly constant. This trend can be rationalized by considering the incremental increase in the effective nuclear charge going from left to right across the third period of elements: as the effective nuclear charge increases, the orbitals experience a net contraction and stabilization in energy. Using the MM-based δ orbitals as a reference, we see that their energy decreases from -5.09 eV for Mo_2 to -5.55 eV for Tc_2 and -6.59 eV for Rh_2. The opposite trend, however, is observed upon moving from Mo_2 to W_2. There is an increase in the δ orbital energy (-4.66 eV) for $W_2(O_2CH)_4$ relative to its Mo_2 analogue, a phenomenon that is well-known.[52]

One of the most interesting aspects of this study are those systems containing Ru_2 metal centers. Experimental and computational evidence have shown the $Ru_2(O_2CR)_4$ (R = various alkyl groups) paddle wheel complexes to be paramagnetic with two unpaired electrons,[68,70] while a series of $[Ru_2]_4$ formamidinate squares, recently characterized by Cotton and co-workers, possess 12 unpaired electrons.[11] With these observations in mind, we performed spin-unrestricted calculations on each system containing Ru_2 centers. To make a comparison with the other MM systems more meaningful, the energy eigenvalues of the α- and β-spin orbitals from the calculations on $Ru_2(O_2CH)_4$, $[(HCO_2)_3Ru_2]_2(\mu\text{-}O_2CCO_2)$, and $[(HCO_2)Ru_2]_4(\mu\text{-}O_2CCO_2)_4$ were averaged. It should be noted that the average energy of the frontier MOs for the $Ru_2(O_2CH)_4$ complex follows the periodic trend upon moving from Mo to Rh across the second row transition metal series (Figure 3).

The filling order of the MM-based MOs in the $M_2(O_2CH)_4$ systems (M = Mo, W, Tc, Ru, and Rh) has long been known, and our computational results are of no great surprise with respect to that (Table 2). They do, however, show how the irreducible representations spanned by the MM-based orbitals fill with progression from $M_2 \rightarrow [M_2]_2 \rightarrow [M_2]_4$ complexes. Our calculations predict a $\sigma^2\pi^4\delta^2\delta^{*0}\pi^{*0}\sigma^{*0}$ configuration for the d^4-d^4 cases where M = Mo and W. For the d^5-d^5 case where M = Tc, the filling is calculated as $\sigma^2\pi^4\delta^2\delta^{*2}\pi^{*0}\sigma^{*0}$; the addition of 2 more electrons to the MM unit necessitates the filling of the MM-based δ^* orbital.

An interesting phenomenon is seen in the cases where M = Ru and Rh. In these instances, the MM-based π^* orbital drops in energy below the δ^* orbital. This change in orbital ordering has been attributed to interactions between the MM δ^* orbital of b_{1u} symmetry with oxygen lone pair orbitals of the same symmetry on the formate ligands.[57] These interactions form the foundation for bonding and antibonding interactions between the MM δ^* orbital and the oxygen lone pairs; the δ^* MO of the $M_2(O_2CH)_4$ complex is, in fact, the antibonding combination with the formate oxygen lone pairs. There is a stronger oxygen lone pair interaction with the MM δ^* orbital in Ru and Rh than that in their second row predecessors; this pushes the δ^* MO of the complex above that of the MM π^* orbital, with the effect that the π^* orbital appears to "drop" in energy. This explanation is enforced by examining the percent contributions of atomic orbitals to the δ^* MOs in the Tc_2, Ru_2, and Rh_2 complexes. A Mulliken population analysis[71] reveals that the δ^* MO in the Tc_2 complex is 83% Tc d_{xy} and 16% oxygen lone pair in character. For the Ru_2 and Rh_2 complexes, however, the δ^* MO is predicted to be 78% Ru d_{xy} and 18% O lone pair in character and 74% Rh d_{xy} and 25% oxygen lone pair in character, respectively. The electron occupations for these d^6-d^6 and d^7-d^7 systems are therefore calculated to be $\sigma^2\pi^4\delta^2\pi^{*2}\delta^{*2}\sigma^{*0}$ and $\sigma^2\pi^4\delta^2\pi^{*4}\delta^{*2}\sigma^{*0}$, respectively.

With the results for these "simple" systems in hand, we can now probe the effect that coupling two MM units through an oxalate bridge has on the electronic structure of MM multiply bonded complexes.

(70) Chisholm, M. H.; Christou, G.; Folting, K.; Huffman, J. C.; James, C. A.; Samuels, J. A.; Wesemann, J. L.; Woodruff, W. H. *Inorg. Chem.* **1996**, *35*, 3643.
(71) Mulliken, R. S. *J. Chem. Phys.* **1955**, *23*, 1833.

Table 2. Filling Order of Formate Model Complexes Considered in This Study

M_2 center	filling of frontier molecular orbitals		
	$M_2(O_2CH)_4$	$[(HCO_2)_3M_2]_2(\mu\text{-}O_2CCO_2)$	$[(HCO_2)M_2]_4(\mu\text{-}O_2CCO_2)_4$
Mo, W	$\sigma^2\pi^4\delta^2\delta^{*0}\pi^{*0}\sigma^{*0}$	$\sigma^4\pi^8\delta^4\delta^{*0}\pi^{*0}\sigma^{*0}$	$\sigma^8\pi^{16}\delta^8\delta^{*0}\pi^{*0}\sigma^{*0}$
Tc	$\sigma^2\pi^4\delta^2\delta^{*2}\pi^{*0}\sigma^{*0}$	$\sigma^4\pi^8\delta^4\delta^{*2}\pi^{*0}\sigma^{*0}$	$\sigma^8\pi^{16}\delta^8\delta^{*8}\pi^{*0}\sigma^{*0}$
Ru	$\sigma^2\pi^4\delta^2\pi^{*2}\delta^{*2}\sigma^{*0}$	$\sigma^4\pi^8\delta^4\pi^{*4}\delta^{*4}\sigma^{*0}$	$\sigma^8\pi^{16}\delta^8\pi^{*8}\delta^{*8}\sigma^{*0}$
Rh	$\sigma^2\pi^4\delta^2\pi^{*4}\delta^{*2}\sigma^{*0}$	$\sigma^4\pi^8\delta^2\pi^{*8}\delta^{*4}\sigma^{*0}$	$\sigma^8\pi^{16}\delta^8\pi^{*16}\delta^{*8}\sigma^{*0}$

Table 3. Irreducible Representations Spanned by the Oxalate π Orbitals in $[(HCO_2)_3M_2]_2(\mu\text{-}O_2CCO_2)$ (D_{2h}) and $[(HCO_2)M_2]_4(\mu\text{-}O_2CCO_2)_4$ (D_{4h})[a]

oxalate π orbitals	$[M_2]_2$ (D_{2h})	$[M_2]_4$ (D_{4h})
π_1	b_{2u}	$a_{1g} + b_{1g} + e_u$
π_2	b_{3g}	$a_{2g} + b_{2g} + e_u$
π_3	b_{1g}	$a_{2u} + b_{2u} + e_g$
π_4	a_u	$a_{1u} + b_{1u} + e_g$
π_5	b_{2u}	$a_{1g} + b_{1g} + e_u$
π_6	b_{3g}	$a_{2g} + b_{2g} + e_u$

[a]A pictorial representation of the six π orbitals appears in Figure 5.

***D_{2h}*-$[(HCO_2)_3M_2]_2(\mu\text{-}O_2CCO_2)$ Dimers of Dimers.** The frontier MOs of the planar oxalate anion are the six π orbitals shown in Figure 5; they transform under D_{2h} symmetry as shown in Table 3. The π_1 and π_2 orbitals are strongly C−O π bonding, while π_3 and π_4 are nonbonding oxygen lone pair orbitals. The LUMO of $O_2CCO_2^{2-}$ is π_5 which is C−O π antibonding and C−C π bonding.

When two MM units are linked together by the oxalate bridge in a planar D_{2h} structure, as in the model compound $[(HCO_2)_3M_2]_2(\mu\text{-}O_2CCO_2)$, the metal-based frontier MOs combine as two sets of σ and σ^*, four π and four π^*, and two δ and two δ^* MOs. As shown in Tables 1 and 3, there are many symmetry-allowed interactions between the MM-based orbitals and the oxalate π-based orbitals. However, only MM δ orbitals of b_{3g} and b_{2u} symmetry have been found, through calculations, to interact significantly with the π_2 and π_5 MOs of oxalate; the most significant interaction involves π_5, the oxalate LUMO. A qualitative MO fragment diagram for $[(HCO_2)_3Mo_2]_2(\mu\text{-}O_2CCO_2)$ is shown in Figure 6 to illustrate these interactions.

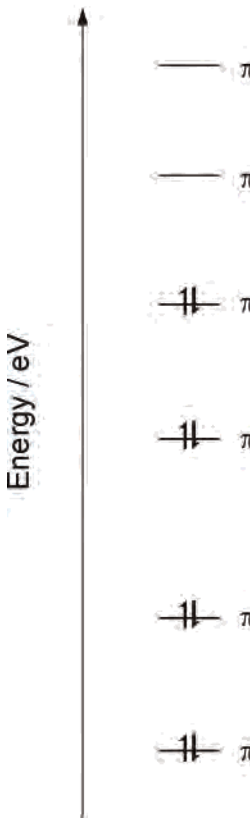

Figure 5. Qualitative molecular orbital diagram and calculated molecular orbital isosurfaces for the oxalate^{2-} anion (isosurface cutoff value = 0.04).

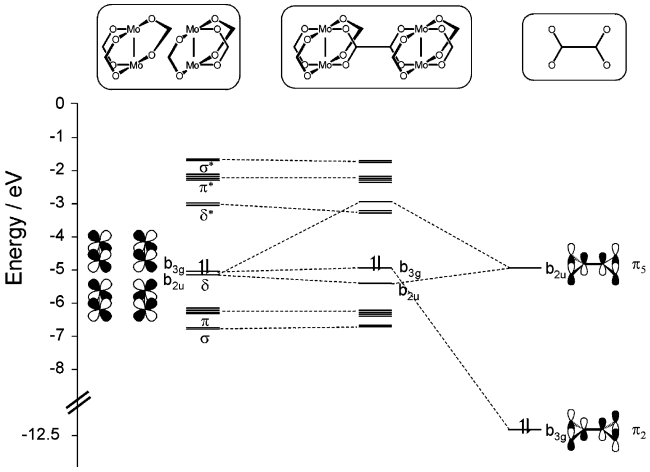

Figure 6. Qualitative MO diagram showing the formation of $[(HCO_2)_3M_2]_2(\mu\text{-}O_2CCO_2)$ from interactions of the frontier orbitals of a $[Mo_2]_2$ fragment with oxalate π orbitals. Splitting of the δ orbitals via symmetry-allowed combinations is attributed to a filled−filled interaction (δ orbital of b_{2u} symmetry with oxalate π_2) and a filled−empty interaction (δ orbital of b_{3g} symmetry with oxalate π_5).

Apart from prior work in this laboratory on the Mo and W derivatives of D_{2h}-$[(HCO_2)_3M_2]_2(\mu\text{-}O_2CCO_2)$ complexes, no theoretical investigations have been performed on related $[M_2]_2$-oxalate-bridged systems (M = Tc, Ru, Rh).[5,20] The general trends that emerge from these calculations are summarized in the molecular orbital energy level diagrams depicted in Figures 7 and 8. In traversing the second row from molybdenum to rhodium, we can readily see the stabilization of the metal-based orbitals and, furthermore, the tightening of the d-block orbital manifold with increasing d^n electron count. The calculations for the heavy element tungsten parallels what is seen for molybdenum and technetium; the major differences are the relative energies of the metal-based orbitals (ca. 0.5 eV higher in energy with respect to their second row congeners).

The cases of the d^4 $[M_2]_2$ complexes (M = Mo and W) have been discussed in detail before and, therefore, do not warrant specific attention beyond noting the following. The δ orbitals are split by symmetry-allowed interactions with π_2 and π_5 (vide supra) of the oxalate bridge (Figure 6). The greater splitting of the δ orbitals for tungsten (ca. 0.6 eV

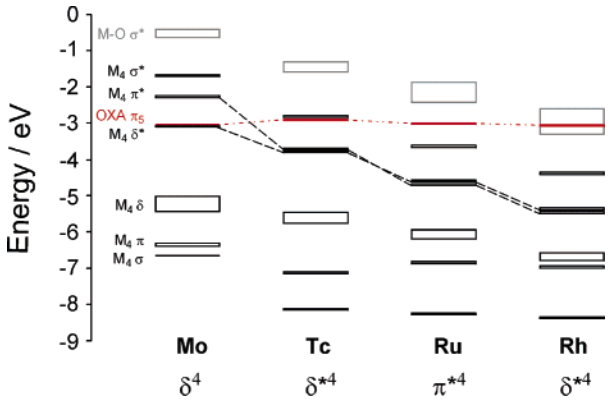

Figure 7. Frontier MO diagrams for second row transition metal $[(HCO_2)_3M_2]_2(\mu\text{-}O_2CCO_2)$ complexes (M = Mo, Tc, Ru, or Rh). The occupation of the HOMO MOs is indicated below the metal of interest. Note the crossing of the δ^* and π^* MOs upon moving from Tc to Ru (see text).

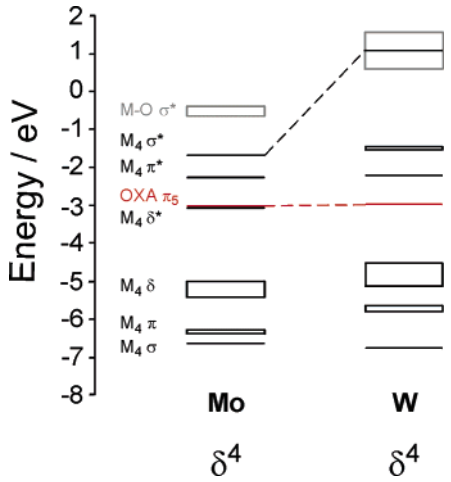

Figure 8. Frontier MO diagram for the third row transition metal complex $[(HCO_2)_3W_2]_2(\mu\text{-}O_2CCO_2)$ as compared to that of $[(HCO_2)_3Mo_2]_2(\mu\text{-}O_2CCO_2)$. The occupation of the HOMO MOs is indicated below the metal.

relative to 0.4 eV for molybdenum) reflects the fact that the $[W_2]_2$ δ combinations are closer in energy to the oxalate π_5 and, therefore, experience a greater orbital overlap.

The d^5 case for M = Tc reveals that the $[M_2]_2$ π^* orbitals drop below the oxalate π_5 and indeed are close in energy to the $[M_2]_2$ δ^* MO. The calculations predict a closed shell configuration with the two highest-filled MOs being the δ^* MOs. While the two $[M_2]_2$ δ^*-based MOs have the correct symmetries to interact with filled oxygen lone pair orbitals on oxalate, there is little mixing with the π orbitals, leaving the two δ^* MOs virtually isoenergetic (vide infra). The occupied $[M_2]_2$ δ MOs with b_{3g} and b_{2u} symmetries are again split by symmetry-allowed and energetically favorable interactions with oxalate π_2 and π_5. The difference in energy between the b_{2g} and b_{3u} δ orbitals is ca. 0.3 eV for Tc. It should be noted that the magnitude of the splitting for $[Tc_2]_2$ is less than that for $[Mo_2]_2$ because of stabilization and contraction of the δ orbitals, from the increased electronegativity of Tc.

For M = Ru, the d^6 case, spin-unrestricted calculations were performed. On the basis of the results for the $Ru_2(O_2CH)_4$ system, the calculation was performed assuming four unpaired electrons in the oxalate-bridged complex, which corresponds to two unpaired electrons for each Ru_2 unit. This assumption manifests itself quite nicely in the results for both the $[Ru_2]_2$ dimer and the $[Ru_2]_4$ square, where there is a foundation in experimental work (vide infra).

As in the case of $Ru_2(O_2CH)_4$, we have averaged the energy eigenvalues of the α- and β-spin orbitals in order to present a meaningful comparison to the other complexes in Figure 7. There are significant changes in the relative ordering of the $[M_2]_2$-based MOs, a phenomenon that echoes the simpler $Ru_2(O_2CH)_4$ case. The $[M_2]_2$ π^* orbitals are stabilized relative to the $[M_2]_2$ δ^* combinations. Even the $[M_2]_2$ σ^* orbitals are now lower in energy than the oxalate π_5-based MO. The HOMO and HOMO-1 are $[M_2]_2$ δ^* combinations and are filled, but the $[M_2]_2$ π^* block of four MOs is only half filled. The fact that the four unpaired electrons occupy the $[M_2]_2$ π^* block complements the half-filled π^* block of the MM dimer, and this allows us to predict that extended structures containing $[Ru_2]_2$ units may mimic the same filling order.

For d^7 Rh(II), the stabilization of the $[M_2]_2$-based orbitals is continued. The $[M_2]_2$ π^* and δ^* orbitals are close in energy and completely filled; the HOMO and HOMO-1 are $[M_2]_2$ δ^* combinations. The LUMO and LUMO$+1$ are $[M_2]_2$ σ^* combinations and have $[M_2]_2-O$ σ^* character (derived from both the metal $d_{x^2-y^2}$ and d_{z^2} orbitals); they are calculated to be lower in energy than the oxalate π_5-based MO. The splitting of the two filled $[M_2]_2$ δ combinations is now quite small (ca. 0.2 eV) as these orbitals are significantly stabilized at ca. -6.7 eV; interestingly, they are comparable in energy to the $[Mo_2]_2$ σ-bonding MOs (Figure 7).

In presenting the summary shown in Figures 7 and 8, we have omitted the oxalate π_2-based MO that interacts with the b_{3g} $[M_2]_2$ δ combination. The oxalate π_2-based orbital is very low in energy (ca. -12 eV) relative to the frontier MOs shown. The oxalate π_3 and π_4 MOs, of b_{1g} and a_u symmetries, respectively, are also very low in energy (ca. -10 eV) and thus have a negligible effect on the $[M_2]_2$ δ^* and π^* combinations (Table 1).

***D*$_{4h}$-[(HCO$_2$)$_2$M$_2$]$_4$(μ-O$_2$CCO$_2$)$_4$ Molecular Squares: An Electronic Property Gedanken Experiment.** For the molecular squares of formula $[(HCO_2)_2M_2]_4(\mu\text{-}O_2CCO_2)_4$, the situation is not so simple. In this case, more of the $[M_2]_4$ and $(O_2CCO_2)_4$ π orbitals transform as the same irreducible representation within the D_{4h} point group (Table 1). For the d^4 cases (M = Mo, W), it is easy to anticipate that the highest-occupied MOs will be derived from the MM δ combinations and that the lowest-lying MOs will be from either the MM δ^* orbitals or from the π_5 orbital of oxalate (Figure 5) because these are the frontier orbitals in the oxalate-bridged dimers. A qualitative MO fragment diagram for $[(HCO_2)_2M_2]_4(\mu\text{-}O_2CCO_2)_4$ is shown in Figure 9. Model complexes of D_{2h}-$[(HCO_2)_3M_2]_2(\mu\text{-}O_2CCO_2)$ and D_{4h}-$[(HCO_2)\text{-}M_2]_4(\mu\text{-}O_2CCO_2)_4$ (M = Mo, W) have also been the subject of computational investigations in this laboratory.[5,20]

The synthesis of molecular squares of the type shown in Figure 1 poses an interesting challenge in the chemistry of carboxylate-ligated MM systems. Carboxylate-based paddle wheel complexes are subject to ligand scrambling, and this

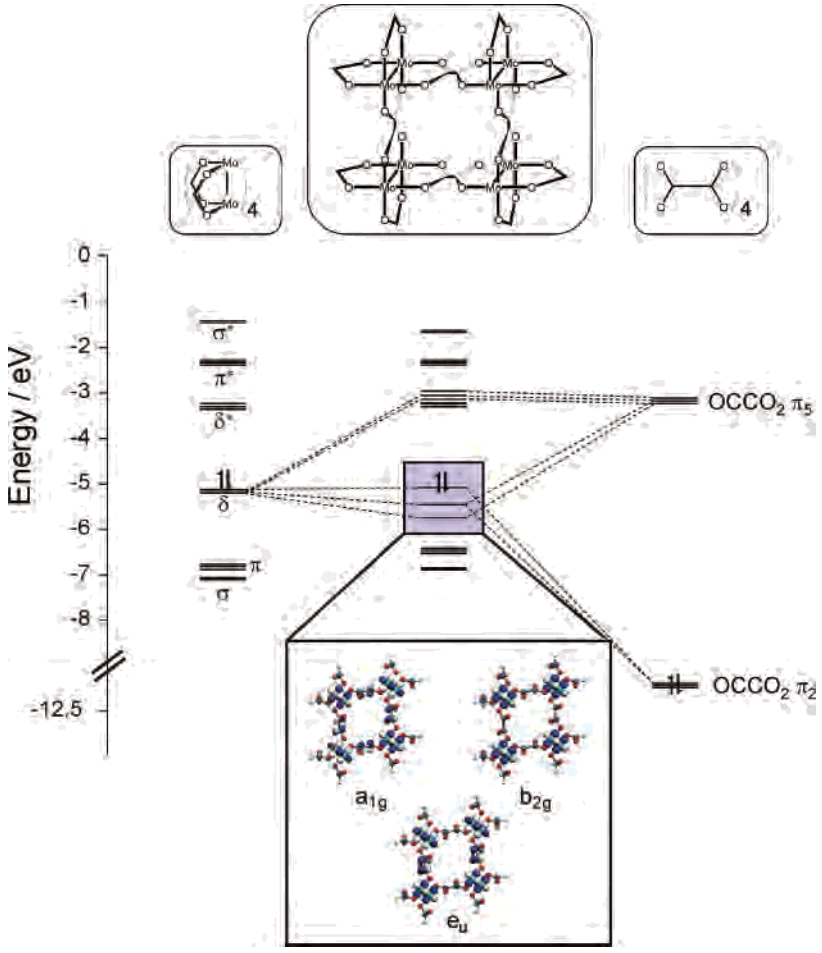

Figure 9. Qualitative MO diagram showing the formation of $[(HCO_2)_2M_2]_4(\mu\text{-}O_2CCO_2)_4$ from interactions of the frontier orbitals of a $[Mo_2]_4$ fragment with oxalate π orbitals. As in the oxalate-bridged dimer of dimers, the δ orbitals split via symmetry-allowed combinations with the oxalate π_2 and π_5 group orbitals. MO isosurface plots for the filled orbitals composing the HOMO are shown (isosurface cutoff value = 0.04). They are, from lowest to highest energy, a_{1g}, e_u, and b_{2g}. Only one e_u orbital is shown for clarity.

effect is exacerbated when one attempts to synthesize square complexes.[18,19,24,72] The electronic properties of these squares promise to be very interesting, which makes investigation of their electronic structure fruitful for future synthetic studies. The frontier MO diagrams for a series of D_{4h}-$[(HCO_2)M_2]_4(\mu\text{-}O_2CCO_2)_4$ complexes (M = Mo, W, Tc, Ru, Rh) are shown in Figures 10 and 11. The general electron filling order of each of these complexes follows the same progression as that seen when going from the simple $M_2(O_2CH)_4$ dimers to the $[(HCO_2)_3M_2]_2(\mu\text{-}O_2CCO_2)$ dimers of dimers and will not be discussed in detail. The most striking feature of these diagrams is that they are a realization of the logical progression of $M_2 \rightarrow [M_2]_2 \rightarrow [M_2]_4$. As the MM centers are incorporated into oligomeric square motifs, the MO structure of the complexes becomes less discrete and more bandlike in character. The consequence of this progression from discrete unit to oligomeric motif is illustrated in Figure 12. While the aforementioned statement by no means implies we are dealing with band structures, it does emphasize what electronic structures would be realized by incorporating MM multiple bonds into 1-D wires (MM centers linked in infinite chains by oxalate) or, in this case, 2-D extended structures (a sheet composed of oxalate-bridged molecular squares). The metal incorporated into this structural motif will greatly impact the electronic properties of the complexes.

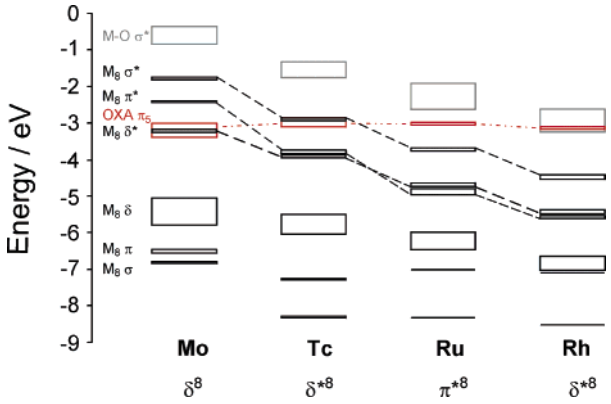

Figure 10. Frontier MO diagrams for second row transition metal $[(HCO_2)_2M_2]_4(\mu\text{-}O_2CCO_2)_4$ complexes (M = Mo, Tc, Ru, or Rh). The occupation of the HOMO is indicated below the metal of interest. Note the crossing of the δ^* and π^* MOs upon moving from Tc to Ru (see text).

In general, the mixing of the $[M_2]_2$ (M = Mo, W) δ orbitals with ligand bridge orbitals of the same symmetry is the foundation for the electronic communication observed between bridged dimetal units. The experimental manifesta-

(72) Chisholm, M. H. C.; MacIntosh, A. M. *J. Chem. Soc., Dalton Trans.* **1999**, 1205.

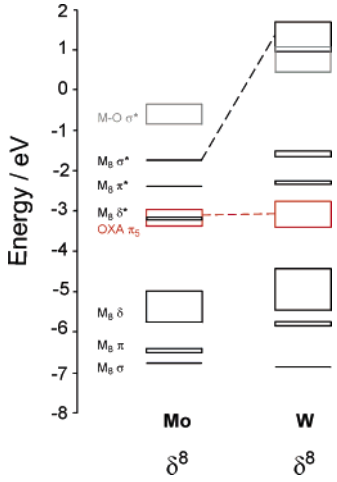

Figure 11. Frontier MO diagrams for the third row transition metal complex $[(HCO_2)_2W_2]_4(\mu\text{-}O_2CCO_2)_4$ as compared to that of $[(HCO_2)_2Mo_2]_4(\mu\text{-}O_2CCO_2)_4$. The occupation of the HOMO MOs is indicated below the metal.

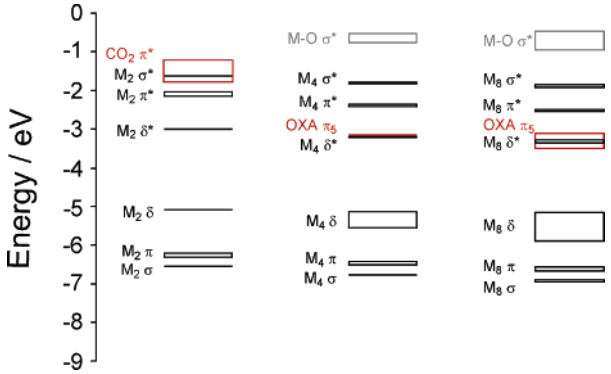

Figure 12. Comparison of schematic MO diagrams showing the "building up" of the molecular orbitals into bandlike structures upon going from $M_2 \rightarrow [M_2]_2 \rightarrow [M_2]_4$ (M = Mo).

tion of this phenomenon has been readily seen in electrochemical, UV−vis, and electron paramagnetic resonance studies on numerous $[M_2]_2$-bridged systems (vide supra). By extending what is known about bridged dimers of dimers to the computational results for squares, we can make reasonable arguments as to which of the $[(HCO_2)M_2]_4(\mu\text{-}O_2CCO_2)_4$ model complexes will exhibit better electronic communication between dimetal centers.

In the case of d^4 $[M_2]_4$ (M = Mo, W), we see that, as before, the greatest orbital interactions are those that occur between the metal δ and the oxalate π_5 MOs. This interaction proves to be particularly important in terms of electronic communication, as the HOMO in these cases is a mix of $[M_2]_4$ δ and oxalate bridge character. The delocalization among the four M_2 fragments could manifest as interesting properties for partially oxidized tetrameric systems (e.g., $[M_2]_4^{q+}$). While the degree of delocalization cannot be well quantified without experimental techniques, it is known that one-electron oxidized species of $[Mo_2]_2$- and $[W_2]_2$-bridged complexes exhibit delocalization across the bridge, with W exhibiting better delocalization. It would thus appear that Mo and W would be excellent choices for metals in extended *n*-dimensional systems.

The fact that Mo and W make good choices as metals to be incorporated into oxalate-bridged square arrays is not accidental. The δ orbitals that comprise the HOMO band in these systems are split by favorable energetic and symmetric interactions with the oxalate bridge π_2 and π_5 MOs (Figure 9). The degree to which the four δ-based orbitals are split (ca. 0.75 eV dispersion between the lowest and highest in the set) illustrates the strong interaction with the oxalate-bridge MOs. The breadth of this energetic splitting has significant implications when considering the electronic structure of $[Mo_2]_n$ or $[W_2]_n$ extended systems. For the *n*-dimensional cases, we would expect disperse valence bands composed of Mo_2 or W_2 MO character mixed with oxalate-bridge π_2 and π_5 character. Whether it be $[M_2]_4$ or $[M_2]_n$ (M = Mo or W), one thing remains certain, the dispersity of the orbitals composing the δ HOMO band is a clear indication of the amount of the contribution of the oxalate-bridge MO character, which in turn dictates the amount of delocalization one would expect between M_2 centers.

The case of d^5 for M = Tc is the first example where we might expect poor electronic communication between M_2 centers. The HOMO for the square complex with this metal is primarily $[M_2]_4$ δ*-based. There is no oxalate-bridge contribution to this orbital or to any of the orbitals which compose the δ* set of MOs. Indeed, there are no oxalate MOs with which find both a favorable symmetric and energetic match with the occupied δ* MOs. This feature, coupled with the observation that the MOs in the δ* set are nearly isoenergetic with virtually no energetic dispersion, illustrates the lack of electronic communication among the four M_2 centers. In the case of both the $[Tc_2]_4$ square and the $[Tc_2]_n$ extended systems, we would therefore expect very narrow valence bands through which electron delocalization would be minimal.

For the d^6 and d^7 cases for M = Rh and M= Ru, respectively, we again expect poor electronic coupling between M_2 centers, as in the case of M = Tc. For M = Ru, the HOMO is $[M_2]_4$ π*, while for M = Rh, the HOMO is $[M_2]_4$ δ*. In both cases, there is no oxalate MO character contributing to the orbitals in the π* or δ* set. The observation for these systems is again similar to that made for technetium, and we would expect poor electronic coupling between the M_2 units.

It is interesting to note that the $[Ru_2]_4$ square frontier MOs show a half-filled set of $[M_2]_4$ π*-based orbitals, suggesting that the system has 8 unpaired electrons. This computational result finds some validation with the previously mentioned $[Ru_2]_4^{5+}$ system synthesized by Cotton and co-workers. In that system, the ancillary carboxylate ligands have been replaced by *N*,*N*′-di(*p*-anisyl)-formamidine (DAniF); the Ru_2 units are ligated by a chloride anion, and the bridging ligands are either oxalate or terephthalate. Magnetic data, coupled with the knowledge that an Ru_2^{5+} unit has a $\sigma^2\pi^4\delta^2\pi^{*2}\delta^{*1}$ electronic configuration, strongly suggest that the system has 12 unpaired electrons.[11]

Conclusions

With the aid of density functional theory calculations, we have determined the electronic structures of $M_2(O_2CH)_4$, $[(HCO_2)_3M_2]_2(\mu\text{-}O_2CCO_2)$, and $[(HCO_2)_2M_2]_4(\mu\text{-}O_2CCO_2)_4$ (M = Mo, W, Tc, Ru, Rh) oxalate-bridged complexes. Upon building up the number of MM units following the progression $M_2 \rightarrow [M_2]_2 \rightarrow [M_2]_4$, it is readily seen that the frontier MOs begin to approximate a bandlike structure from which we can start to anticipate the properties of an extended 2-D grid. The implications are that materials with MM units should exhibit interesting electronic properties as they are incorporated into an extended structure. With this implication, however, there is a caveat. Only those systems with M = Mo or W should exhibit electron delocalization mediated by the oxalate bridge. These systems should have a valence band dispersion on the order of 1 eV. Oxidation should be relatively easy and, from an energetic standpoint, could lead to metallic-like conductivity. The same type of mixing is not seen in bridged complexes for M = Tc, Ru, and Rh. The HOMO orbitals of complexes with the aforementioned metals are primarily metal-based and, in an extended lattice, would lead to a very narrow metal-based band. Oxidation would not be expected to result in good conductivity.

While oxalate is a good bridge for mediating electronic communication between MM centers, it is not one that has found synthetic utility for extended gridlike structures, nor can it be modified. The incorporation of MM units into extended materials has been achieved with other conjugated organic bridges (i.e., phenyl and thienyl dicarboxylate bridges), and these aromatic systems lend themselves to further electronic modification. However, it follows from the present study of oxalate that the greatest electronic coupling between M_2 units will be for molybdenum and tungsten where the filled metal δ orbitals are of highest energy.

Acknowledgment. The authors gratefully acknowledge support from the National Science Foundation and the Ohio Supercomputing Center for computational resources. J.S.D. gratefully acknowledges Professors Christopher Hadad and Patrick Woodward for fruitful discussions. He also acknowledges Ms Constance Brett and Mr. Jason Sonnenberg for helpful ideas and computational assistance.

Supporting Information Available: Optimized coordinates of model complexes. This material is available free of charge via the Internet at http://pubs.acs.org.

IC050053N